Electronic Supplementary Material (ESI) for Journal of Materials Chemistry C.

Supporting Information

Elucidating Charge Transport Mechanisms in Cellulose-Stabilized Graphene Inks

Ana C. M. de Moraes,‡[a] Jan Obrzut,*‡[b] Vinod K. Sangwan,[a] Julia R. Downing,[a] Lindsay E. Chaney,[a] Dinesh K. Patel,[c] Randolph E. Elmquist,[c] and Mark C. Hersam*[a,d,e,f]

[a] Department of Materials Science and Engineering, Northwestern University, Evanston, IL 60208, USA

[b] Materials Science and Engineering Division, Material Measurement Laboratory, National Institute of Standards and Technology, Gaithersburg, MD 20899, USA

[c] Quantum Measurements Division, Physical Measurement Laboratory, National Institute of Standards and Technology, Gaithersburg, MD 20899, USA

[d] Department of Chemistry, Northwestern University, Evanston, IL 60208, USA

[e] Department of Medicine, Northwestern University, Evanston, IL 60208, USA

[f] Department of Electrical and Computer Engineering, Northwestern University, Evanston, IL 60208, USA

‡ These authors contributed equally to this work.

*E-mails: jan.obrzut@nist.gov (J.O.) and m-hersam@northwestern.edu (M.C.H.)

Materials

Graphene Exfoliation and Characterization

In a pilot-scale exfoliation process, 6 kg of flake graphite (Sigma-Aldrich) were dispersed in a solution of ethyl cellulose (EC, 4×10^{-3} Pa·s, Sigma-Aldrich) in ethanol with a 30:1:20 weight ratio. This process mixture was continuously recirculated for 23 h in a Silverson 200L high-shear, inline configuration. The shear-mixed dispersion was centrifuged at 680.67 rad/s for 30 min (Avanti J26-XPI centrifuge, JLA 8.1000 rotor, Beckman Coulter) to crash out unexfoliated graphite flakes. The supernatant containing the exfoliated graphene nanosheets stabilized with EC was removed and flocculated with a 40 g/L sodium chloride (NaCl, Sigma-Aldrich) aqueous solution in a 16:9 weight ratio (Gr/EC dispersion:NaCl solution). This mixture was then centrifuged at 733.04 rad/s for 7 min to isolate the Gr/EC flocs and to remove excess polymer binder. The residual salt was removed by flushing deionized water over the flocs via a vacuum filtration process, followed by exposure under an infrared lamp (150 W) in ambient conditions for 3 h to dry the exfoliated Gr/EC solids. The graphene solids content in the resulting Gr/EC powder was determined by thermogravimetric analysis (TGA), revealing a graphene mass fraction of 49.4 % in the exfoliated powder (Figure S1). The TGA analysis was performed in a Mettler Toledo TGA/SDTA851 instrument in the temperature range from 25 °C to 500 °C with a ramp rate of 0.125 °C/s and a synthetic air flow rate of 8.3×10^{-4} L/s.

Graphene Ink Preparation, Deposition, and Characterization

Graphene ink was prepared by dispersing a mass fraction of 2.0 % Gr/EC powder in a 90:10 mixture of ethanol/ethyl lactate (Sigma-Aldrich) by bath sonication for > 6 h. The dispersion was further filtered through a 1.2 μm glass microfiber syringe filter (Whatman), resulting in a graphene ink with a Gr/EC mass fraction of 2.86 %, as determined by TGA (Figure S2) and

viscosity of 7.0×10^{-3} Pa·s at 1000 s^{-1}. Rheology measurements were carried out in an Anton Paar Physica MCR 302 rheometer using a cone-plate measuring system (diameter = 25 mm, cone angle = 2°) at shear rates from 1 s^{-1} to 1000 s^{-1} at 25 °C.

Graphene films were deposited by blade-coating onto polyimide and undoped silicon wafers over a 300 nm thick SiO_2 insulating layer. Specimens coated on polyimide were cut to 3 mm by 15 mm (width x length) for non-contact microwave cavity measurements while specimens coated on Si/SiO_2 were diced to 7 mm by 7 mm for Hall measurements. The graphene ink was deposited onto the substrate by manually dragging the film applicator (micrometer adjustable EQ-Se-KTQ-50 film casting knife) using a blade gap of 60 μm. The operation was repeated twice to achieve the desired thickness of ≈ 500 nm for the Gr/EC film on a Si/SiO_2 substrate. A blade gap of 40 μm was used for depositing the Gr/EC ink on a polyimide substrate, and the deposition was performed 4 times to achieve a Gr/EC film ≈ 4 μm thick. Both substrates were used as-received and coated at room temperature, producing smooth and homogeneous Gr/EC films. The blade gap was adjusted according to the pristine substrate thickness. The films were allowed to dry at room temperature followed by thermal annealing at 300 °C for 30 min in a tube furnace (Lindberg Blue M, Thermo Fisher Scientific) under ambient conditions in order to decompose the EC polymer from the as-coated Gr/EC films. For further physicochemical analysis and electron microscopy imaging, the same ink was spin-coated to a thickness of ≈ 265 nm on 300 nm SiO_2/Si substrates.

Structural Analysis

Top-view and cross-sectional scanning electron microscopy (SEM) imaging of graphene films were conducted using Hitachi S4800 and SU8030 microscopes, respectively. An accelerating voltage of 5.0 kV was used with a ≈ 4 mm working distance. Raman spectroscopy was conducted using a Raman laser microscope (Horiba LabRAM HR Evolution) equipped with a 532 nm

excitation wavelength laser using an acquisition time of 30 s and 2400 g/mm grating. X-ray photoelectron spectroscopy (XPS) measurements were performed on an ESCALAB 250Xi spectrometer (Thermo Fisher Scientific) equipped with an electron flood gun and a scanning ion gun. The spectra were analyzed using the Thermo Avantage data system.

Hall Measurements

Surface resistance (R_{xx}), density of charge carriers, majority type of charge carriers, and mobility were obtained from magnetoresistance measurements using a conventional 6-terminal Hall Bar configuration.[1] The constant source driving current (I_x) of 1.0 μA was applied between the two source longitudinal terminals while the transverse magnetic field (B_z) was scanned between ± 10 T. The resulting Hall voltage (V_{xy}) was measured between terminals orthogonal to the current directions, while the longitudinal resistance (R_{xx}) was measured between longitudinal terminals along the driving current direction.

Eq. S1 – S3 define the classical relations between the Hall coefficient (R_H) and the corresponding expressions for charge carrier density (n_p) and their mobility (μ):[1,2]

$$R_H = V_{xy}/(I_x B_z) \times (t\ l/w) \qquad \text{(S1)}$$

$$n_p = 1/(q\ R_H) \qquad \text{(S2)}$$

$$\mu = R_H/R_{xx} \qquad \text{(S3)}$$

where*, t, l,* and, *w* are the thickness, length, and, width of the specimen, respectively; $q = 1.6 \times 10^{-19}$ C is the elementary charge; B_z is transverse magnetic field; and V_{xy}, I_x, and R_{xx} are as defined in the main text. In 2D, $t = 1$ and l/w is the aspect ratio of the Hall test structure.

Eq. S1 – S3 can be rearranged to obtain the carrier density and mobility directly from the slope of the Hall voltage versus scanned magnetic field plots:

$$\mu = d(V_{xy}/B_z) \times 1/(I_x R_{xx}) \qquad \text{(S4)}$$

$$n_p = d(V_{xy}/B_z)\,(I_x/q) \qquad \text{(S5)}$$

The magnetoresistance was measured at cryogenic temperatures from 1.5 K to 20 K. The temperature-dependent R_{xx} without magnetic field applied (at $B_z = 0$) was measured during cooling down from 295 K to 1.5 K and then warming up back to 295 K. In the present study, we omit the film thickness as a parameter and present our results for surface charge transport in two dimensions (2D). This approach simplifies the analysis of the experimental results without compromising their physical significance.

Microwave Perturbation Cavity Measurements

Electrical characterization at microwave frequencies was carried out in a parallel experiment at room temperature using a non-contact microwave cavity method operating at the TE_{103} mode.[3] Based on the cavity perturbation method, this non-contact measurement monitors the variation in the quality factor (Q) of the cavity as the specimen is progressively inserted into the cavity in a quantitative correlation with the specimen surface area:

$$\frac{1}{Q_x} - \frac{1}{Q_0} = \sigma_s \frac{2wh_x}{\pi\varepsilon_0 f_x V_0} c_\omega - 2b'' \qquad \text{(S6)}$$

where, σ_s is the surface conductance of graphene ink specimen, ε_0 is the permittivity of free space, Q_x is the quality factor of cavity loaded with the specimen area wh_x, at which the resonant frequency is f_x $c_\omega = (f_x/f_0)^2$ accounts for frequency correction due to substrate polarization and f_0, Q_0, and V_0 are the resonant frequency, quality factor, and volume of the empty (air filed) cavity, respectively. The resonance quality factor is obtained from the resonant peak according to the conventional half power bandwidth formula as $Q_x = f_s / \Delta f_s$, where Δf_s is the bandwidth of the resonant peak. Fig. S7 shows the graphical representation of the cavity perturbation equation (Eq. S6) for our graphene inks at the resonant frequency of 7.435 GHz where intercept b'' is a constant.

From the slope of the plot in Figure S6, we find that the sheet conductance is: $\sigma_s = (9.3 \times 10^{-3} \pm 3 \times 10^{-4})$ S.

Uncertainty analysis

The combined standard uncertainty of the presented charge transport parameters was obtained from the general formula for the error propagation model[5] using standard errors from the least-squares linear fitting through data points or by using maximum errors of the measured values.

In the case of the charge carrier mobility (Eq. S4), the standard error from the linear fit of the slope $d(V_{xy}/B_z) = (-0.01504$ is $\pm 6 \times 10^{-5})$ V/T. The maximum error in $R_{xx} = (95.25 \pm 2)\ \Omega$ and the maximum error in I_x is $(1.0 \times 10^{-6} \pm 50 \times 10^{-9})$ A. Consequently, from Eq. S4 the combined relative uncertainty of mobility $\Delta\mu/\mu$:

$$\Delta\mu/\mu = \text{SQRT}\ [(6 \times 10^{-5}/0.015)^2 + (50 \times 10^{-9}/10^{-6})^2 + (2/95.25)^2] = 0.054\ (5.4\%).$$

Similarly, from Eq. S5 the combined relative uncertainty of charge carrier concentration $\Delta n_p/n_p$:

$$\Delta n_p/n_p = \text{SQRT}\ [(6 \times 10^{-5}/0.015)^2 + 50 \times 10^{-9}/10^{-6})^2] = 0.050\ (5\%).$$

The combined relative uncertainty in surface conductance obtained from the standard error of the least-squares linear fitting to Eq. S6, $\sigma_s = (9.3 \times 10^{-3} \pm 3 \times 10^{-4})$ S and $\Delta\sigma_s/\sigma_s = 0.03$ (3%). Here, we assume that the uncertainty of V_0, f_0, and Q_0 are fixed, that is, these do not affect the slope of the cavity perturbation plot (Fig. 3, main manuscript) over the duration of the measurement cycle and therefore can be neglected in the error propagation model.

Standard errors in reported activation energies in Fig. 4a are obtained from the least-squares linear fitting to the Arrhenius Equation: $ln\ (\sigma_r) = ln(\sigma_0) + E_g/kT$:

$E_{g1} = (4.2 \times 10^{-3} \pm 2.4 \text{ x } 10^{-5})$ eV, $E_{g2} = (5.9 \times 10^{-5} \pm 8.2 \times 10^{-7})$ eV and $E_{g3} = (1.0 \times 10^{-5} \pm 2.1 \times 10^{-8})$ eV.

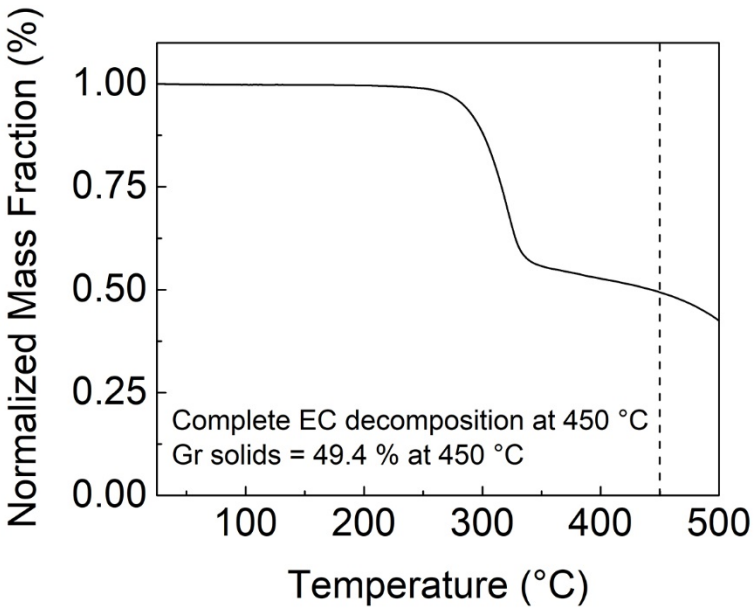

Fig. S1. TGA curve of the graphene/EC powder. The mass fraction of graphene solids was determined after complete decomposition of ethyl cellulose at 450 °C.

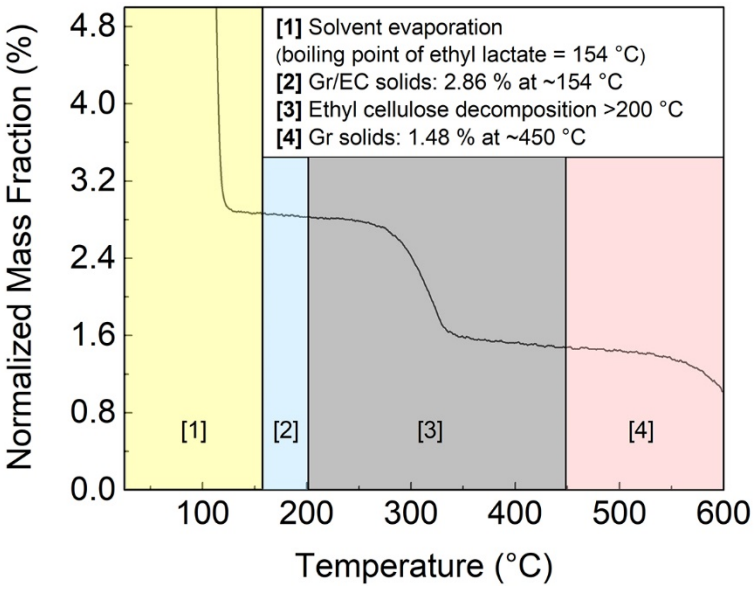

Fig. S2. TGA curve of the graphene ink showing that the ink is composed of 2.86 % graphene/EC solids and 1.48 % graphene after complete EC decomposition above 400 °C.

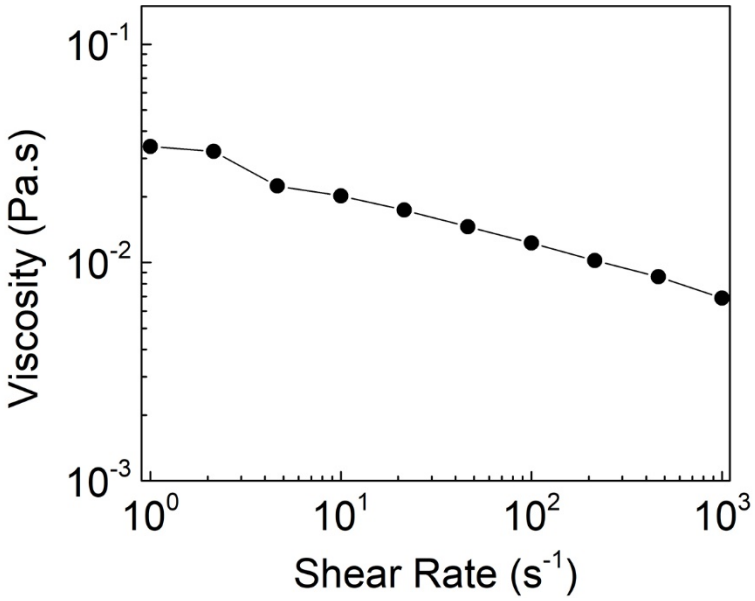

Fig. S3. Viscosity of the graphene ink as a function of shear rate.

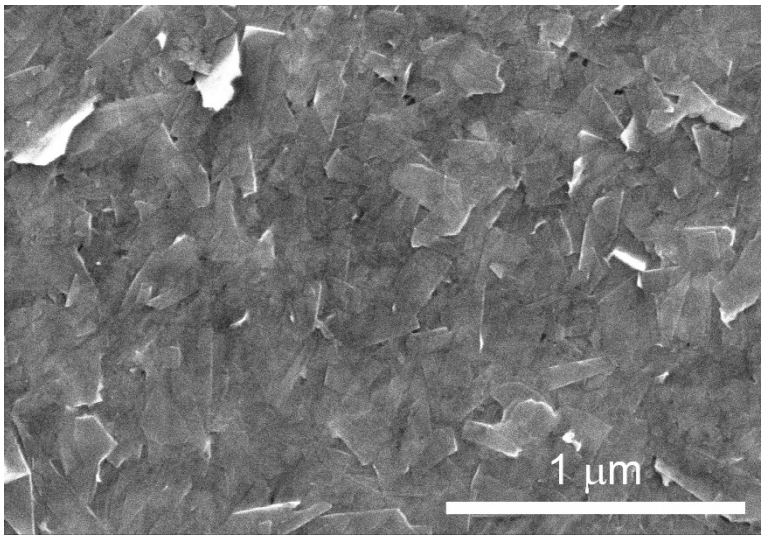

Fig. S4. Top-down SEM image of the graphene film after thermal decomposition of EC (30 min at 300 °C). The image shows a uniform, percolating graphene film.

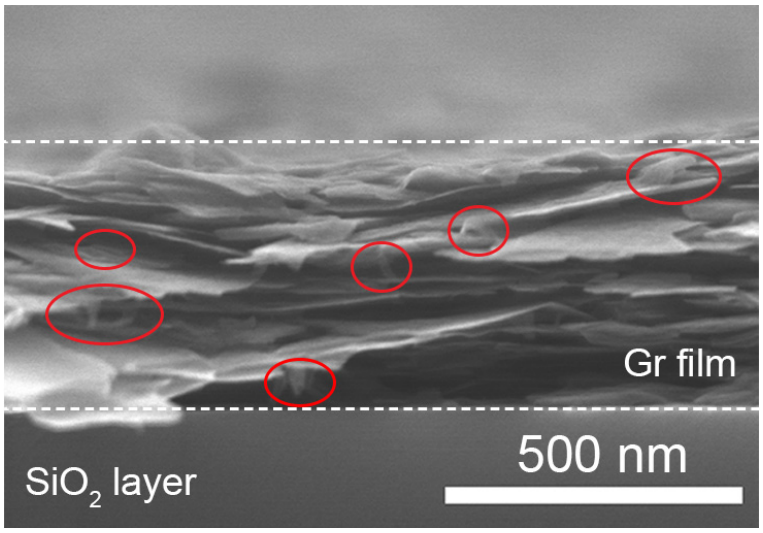

Fig. S5. Higher magnification of the cross-sectional SEM image of the graphene film after thermal decomposition of EC. The image shows evidence of the amorphous carbon residues from the decomposed EC, as indicated by the red circles.

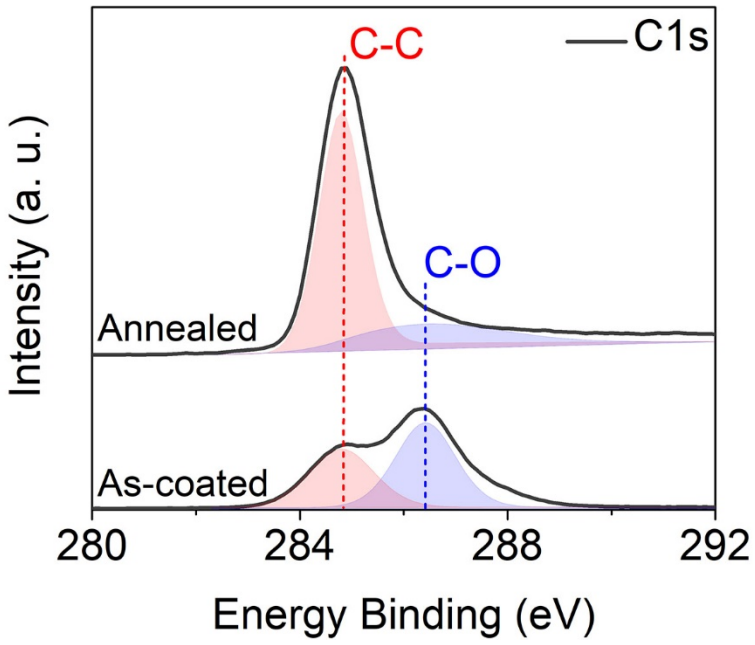

Fig. S6. High-resolution C1s XPS scans of the as-coated graphene film and the graphene film after thermal annealing of EC.

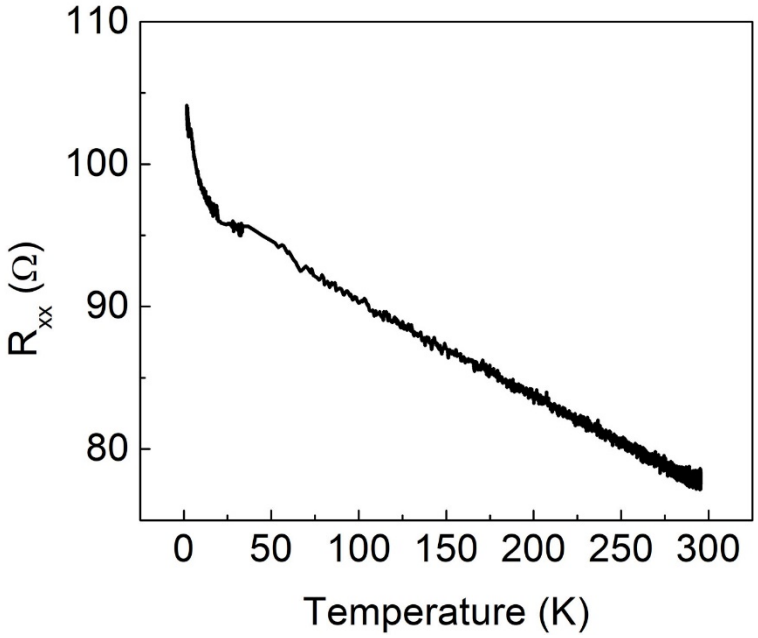

Fig. S7. Temperature dependence of DC longitudinal resistance (R_{xx}).

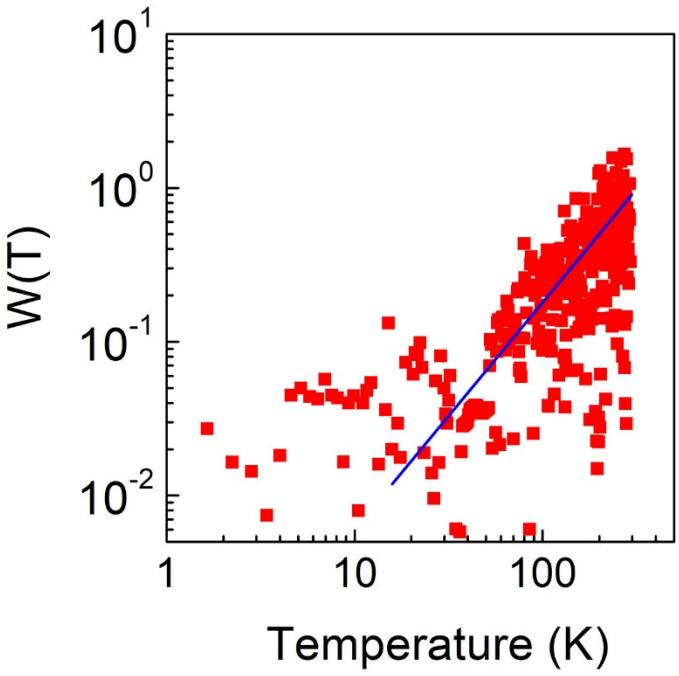

Fig. S8. Temperature dependence of the reduced activation energy (W), $W(T) = -\frac{d(lnR(T))}{d(lnT)}$, showing a decreasing behavior with decreasing temperature, whereas Mott variable-range hopping (VRH) predicts an increasing $W(T)$ to produce non-zero activation energy at zero temperature.[4]

References

1 C. Chien, The Hall effect and its applications, Springer, Science & Business Media, 2013.

2 M. Lundstrom, Resistivity and Hall effect measurements (tutorial) https://nanohub.org/resources/12552/download/2011.10.05-ECE656-L17.pdf

3 J. Obrzut, C. Emiroglu, O. Kirillov, Y. F. Yang and R. E. Elmquist, *Measurement*, 2016, **87**, 146.

4 N. F. Mott, *Metal-Insulator Transitions*, 2nd ed.; Taylor & Francis: London, 1990, 65-105.

5 L. Kirkup, B. Frenkel, *An Introduction to Uncertainty in Measurement*; Cambridge University Press, Cambridge, UK, 2006.